# Dual solutions for MHD flow of a water-based TiO₂-Cu hybrid nanofluid over a continuously moving thin needle in presence of thermal radiation

**Seyed Mehdi Mousavi [1], Mohammadreza Nademi Rostami [1], Mohammad Yousefi [1] and Saeed Dinarvand [1]**

[1] Mechanical Engineering Department, Central Tehran Branch, Islamic Azad University, Tehran, Iran, e-mail: mousavi.sm1976@gmail.com; mr.nr1389@gmail.com; myousefi94@yahoo.com; saeed_dinarvand@yahoo.com.

| Article Info | ABSTRACT |
|---|---|
| | In this analysis, the flow and heat transfer characteristics of an aqueous hybrid nanofluid with TiO2 and Cu as the nanoparticles past a horizontal slim needle in the presence of thermal radiation effect is investigated. We hope that the present research is applicable in fiber technology, polymer ejection, blood flow, etc. The Prandtl number of the base fluid is kept constant at 6.2. The needle is considered thin when its thickness does not exceed that of the boundary layer over it. Using the similarity transformation method, the governing PDEs are transformed to a set of non-linear ODEs. Then, the converted ODEs are numerically solved with help of bvp4c routine from MATLAB. Results indicate that the dual similarity solutions are obtained only when the slim needle moves in the opposite direction of the free stream. In addition, the first solutions are stable and physically realizable. Besides, the second nanoparticle's mass and also the magnetic parameter lead to decrease the range of the velocity ratio parameter for which the solution exists.<br><br> |

*Corresponding Author:*

Saeed Dinarvand,
Mechanical Engineering Department, Central Tehran Branch, Islamic Azad University, Tehran, Iran.
Email: saeed_dinarvand@yahoo.com

## 1. Introduction

The hybrid nanofluids are very new kind of nanofluids, which can be prepared by suspending (i) different types (two or more than two) of nanoparticles in base fluid, and (ii) hybrid (composite) nanoparticles in base fluid. A hybrid material is a substance which combines physical and chemical properties of different materials simultaneously and provides these properties in a homogeneous phase. Synthetic hybrid nanomaterials exhibit remarkable physicochemical properties that do not exist in the individual components (Sarkar et al., 2015). The studies (Ghadikolaei et al., 2017; Yousefi et al., 2018; Dinarvand, 2019; Shojaie Chahregh and Dinarvand, 2020; Ijaz et al., 2018) showed a promising reaction of hybrid nanofluids in heat transfer system, as its thermophysical properties produced a great tendency towards improved heat rate as compared to single nanoparticles. Because hybrid nanofluids showed a promising impact in a heat transfer system, there are still many studies carried out to study the stability and side effects of its implementation in the system. In addition, hybrid nanofluids showed a great reflection towards reactivity and pressure drop characteristics. Moreover, the size of the hybrid nanoparticles, surface adsorption, volume fraction and concentration play a vital role in producing a stable and reactive hybrid nanofluid (Hamzah et al., 2017). Some of the application areas include; heat exchanger, electronic cooling, heat pipes, car radiators, coolant in welding and machining, nuclear plant, solar heating, biomedical applications, drug delivery, etc. (Che Sidik et al., 2016; Gupta et al., 2018). Madhesh

and Kalaiselvam (2014) were experimentally investigated the heat transfer characteristics of a hybrid nanofluid with Cu-TiO2 hybrid nanocomposite using a tube-in-tube counter flow heat exchanger. Results showed that the convective heat transfer coefficient of nanofluids increased with hybrid nanocomposite concentration and Reynolds number. Moldoveanu et al. (2018) presented an experimental study on rheological behavior of hybrid nanofluids made of Al2O3–TiO2 suspended in pure water. Also, a regression analysis was done in order to connect the relative viscosity with volume fractions of both nanofluids and hybrid nanofluid. Recently, Khashi'ie et al. (2020) focused on the three-dimensional hybrid nanofluid flow and heat transfer due to a deformable (stretching/shrinking) plate with power-law velocity and orthogonal surface shear. The effect of adding Cu and Al2O3 nanoparticles are represented by a homogeneous mixture model with the modified thermophysical properties. It is worth mentioning that duality of the similarity solutions are observed in both stretching and shrinking regions, however, only the first solution is proved to be stable and realistic. Semi-analytical modeling of a steady laminar MHD mixed convection incompressible viscous and electrically conducting hybrid nanofluid (CuO-Cu/blood) flow near the plane stagnation-point over a horizontal porous linearly stretching sheet along with a variable magnetic field by a novel computational algorithm according to nanoparticles and base fluid masses were done by Dinarvand et al. (2019). It was proven that when the blade shapes for both nanoparticles are taken into account, the local heat transfer rate is maximum that is also compatible with experimental observations.

An equation governing the motion of an incompressible fluid flowing axially over a thin paraboloid of revolution was initially derived by Lee (1967). Later, Ishak et al. (2007) studied the boundary-layer flow on a moving isothermal slim needle parallel to a moving stream. Their results proved that the dual solutions occur when the needle and the free stream move in the opposite directions. The thin needle has numerous applications in the boundary layer such as fiber technology, polymer ejection, blood flow, coating of wires, transportation, geothermal power generation, etc. (Upreti and Kumar, 2019). Soid et al. (2017) investigated a steady two-dimensional laminar forced convection boundary layer flow along a horizontal slim needle immersed in a Cu/water mono-nanofluid with dual solutions and its stability analysis. The influences of the needle size and the solid volume concentration on the flow and heat transfer characteristics as well as on the velocity and temperature distributions were discussed in details. And Hamid et al. (2019) examined the incompressible MHD flow of graphene oxide/water nanofluid past a continuously moving slim needle with radiation effect plus the dual similarity solutions analysis. The outcomes implied that the flow fields strongly depend on size and shape of the needle and only the upper solution branch (the first solutions) is stable and physically realizable.

Motivated by the above investigations, the present paper considers the dual solutions of laminar steady MHD flow of a TiO2-Cu/water hybrid nanofluid past a moving horizontal thin needle with radiation. A very useful model (called the mass-based model) for hybrid nanofluid's analysis is taken into account. The foregoing model initially uses the mass of both nanoparticles as well as the mass of the base fluid in order to compute the equivalent density, equivalent specific heat and equivalent volume concentration for nanoparticles. Then substituting those five vital relations into governing equations gives us the mass-based single-phase differential equations that we must numerically solve them. The final similarity ordinary differential equations (ODEs) under the relevant boundary conditions are solved with help of bvp4c code in MATLAB. After that, the results and discussion about graphical and tabular findings are presented.

## 2. Mathematical formulation

We consider a steady, laminar MHD boundary layer flow past a continuously moving horizontal slim needle filled with a TiO$_2$-Cu/water hybrid nanofluid along with thermal radiation effect as shown in Fig. 1. We assumed only needles whose thicknesses are comparable to that of the boundary layer or smaller (Lee, 1967). Also, it is assumed that the solid phase and the fluid phase are in thermal equilibrium and no slip occurs between them. Besides, at first the titanium oxide (TiO$_2$) as the first nanoparticle is dispersed in pure water; then the copper (Cu) as the second nanoparticle is suspended in it. The thermophysical properties of the base fluid and nanoparticles are given in Table 1. Under these assumptions and following the nanofluid model proposed by Tiwari and Das (2007) and using the Roseland approximation, the governing equations for the continuity, momentum and energy can be written as (Soid et al., 2017; Hamid et al., 2019).
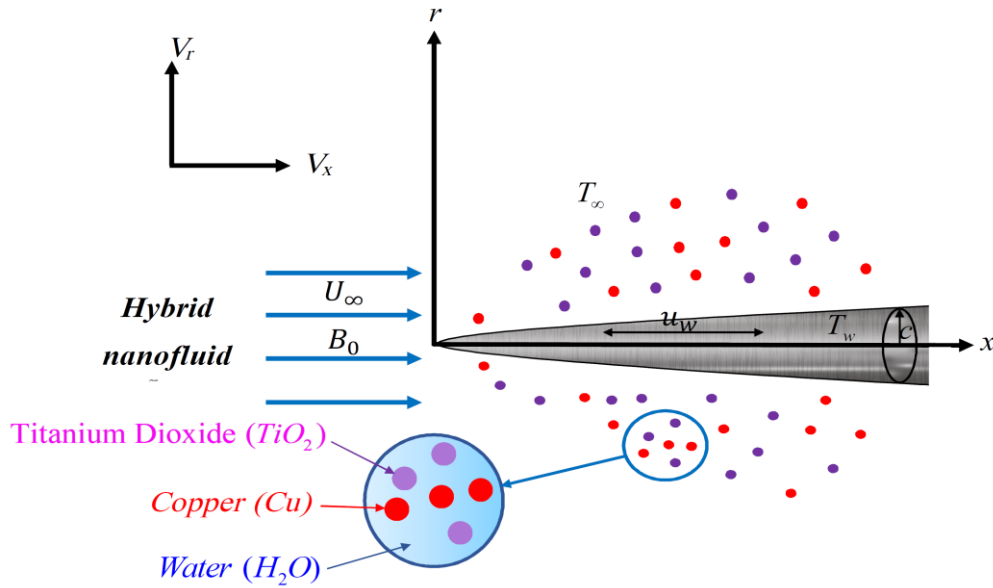
**Figure 1**. Physical view of the problem.

**Table 1.** Thermophysical properties of base fluid and nanoparticles (Sarkar et al., 2015)

| Property | $H_2O$ | $TiO_2$ | $Cu$ |
|---|---|---|---|
| $\rho$ | 997.1 | 4250 | 8933 |
| $C_p$ | 4179 | 686.2 | 385 |
| $k$ | 0.613 | 8.954 | 400 |
| Particle size (in nanometer) | – | 50 | 20 |

$$\frac{\partial}{\partial x}(rV_x) + \frac{\partial}{\partial r}(rV_r) = 0, \tag{1}$$

$$V_x \frac{\partial V_x}{\partial x} + V_r \frac{\partial V_x}{\partial r} = \frac{\mu_{hnf}}{\rho_{hnf}} \frac{1}{r} \frac{\partial}{\partial r}\left(r \frac{\partial V_x}{\partial r}\right) - \frac{\sigma B_0^2 V_x}{\rho_{hnf}}, \tag{2}$$

$$V_x \frac{\partial T}{\partial x} + V_r \frac{\partial T}{\partial r} = \frac{1}{(\rho C_P)_{hnf}}\left[\frac{16\sigma^* T_\infty^3}{3K^*} + k_{hnf}\right]\frac{1}{r}\frac{\partial}{\partial r}\left(r\frac{\partial T}{\partial r}\right), \tag{3}$$

under the boundary conditions [17,18]

$$V_x = u_w, \qquad V_r = 0, \qquad T = T_w, \qquad at \quad r = R(x),$$
$$V_x \to U_\infty, \qquad T \to T_\infty, \qquad as \quad r \to \infty. \tag{4}$$

Further, Table 2 demonstrates the effective thermophysical properties of hybrid nanofluid plus five vital relations for our mass-based model including equivalent density, equivalent specific heat, equivalent volume concentration, volume concentration of first nanoparticle and volume concentration of second nanoparticle in terms of the nanoparticles and base fluid masses (i.e. $w_1$, $w_2$ and $w_f$).

Following Ishak (2007), we introduce the following similarity variables:

$$\eta = \frac{U_0 r^2}{\upsilon_f x}, \qquad\qquad \psi = \upsilon_f x f(\eta), \qquad\qquad \theta(\eta) = \frac{T - T_\infty}{T_w - T_\infty}, \tag{5}$$

Using $V_x = (1/r)(\partial \psi / \partial r)$ and $V_r = (-1/r)(\partial \psi / \partial x)$, and putting Eq. (5) inside Eqs. (1)-(3), we will get:

$$2C_1\left[\frac{d^2f}{d\eta^2}+\eta\frac{d^3f}{d\eta^3}\right]+C_2f\frac{d^2f}{d\eta^2}-M\frac{df}{d\eta}=0, \tag{6}$$

$$2\left(R+\frac{k_{hnf}}{k_f}\right)\left[\frac{d\theta}{d\eta}+\eta\frac{d^2\theta}{d\eta^2}\right]+C_3Prf\frac{d\theta}{d\eta}=0, \tag{7}$$

$$C_1=\left(1-\frac{\frac{m_1}{\rho_1}+\frac{m_2}{\rho_2}}{\frac{m_1}{\rho_1}+\frac{m_2}{\rho_2}+\frac{m_f}{\rho_f}}\right)^{-2.5}, \quad C_2=1-\left(\frac{\frac{m_1}{\rho_1}+\frac{m_2}{\rho_2}}{\frac{m_1}{\rho_1}+\frac{m_2}{\rho_2}+\frac{m_f}{\rho_f}}\right)+\left(\frac{\frac{m_1}{\rho_1}+\frac{m_2}{\rho_2}}{\frac{m_1}{\rho_1}+\frac{m_2}{\rho_2}+\frac{m_f}{\rho_f}}\frac{\rho_s}{\rho_f}\right),$$

$$C_3=1-\left(\frac{\frac{m_1}{\rho_1}+\frac{m_2}{\rho_2}}{\frac{m_1}{\rho_1}+\frac{m_2}{\rho_2}+\frac{m_f}{\rho_f}}\right)+\left(\frac{\frac{m_1}{\rho_1}+\frac{m_2}{\rho_2}}{\frac{m_1}{\rho_1}+\frac{m_2}{\rho_2}+\frac{m_f}{\rho_f}}\frac{(\rho C_p)_s}{(\rho C_p)_f}\right).$$

**Table 2.** Effective thermophysical properties of hybrid nanofluid and five vital mass-based relations (Dinarvand et al., 2019; Dinarvand and Nademi Rostami, 2019; Dinarvand et al., 2019)

| Properties | Thermophysical properties of hybrid nanofluid |
|---|---|
| Dynamic viscosity $(\mu_{hnf})$ | $\dfrac{\mu_f}{(1-\phi_e)^{2.5}}$ |
| Density $(\rho_{hnf})$ | $(1-\phi_e)\rho_f+\phi_e\rho_s$ |
| Volumetric heat capacity $(\rho C_P)_{hnf}$ | $(1-\phi_e)(\rho C_P)_f+\phi_e(\rho C_P)_s$ |
| Thermal conductivity $(k_{hnf})$ | $\dfrac{k_2+2k_{nf}-2\phi_2(k_{nf}-k_2)}{k_2+2k_{nf}+\phi_2(k_{nf}-k_2)}\times k_{nf};$ $k_{nf}=\dfrac{k_1+2k_f-2\phi_1(k_f-k_1)}{k_1+2k_f+\phi_1(k_f-k_1)}\times k_f$ |
| Equivalent density $(\rho_s)$ | $\dfrac{(\rho_1\times m_1)+(\rho_2\times m_2)}{m_1+m_2}$ |
| Equivalent specific heat at constant pressure $((C_P)_s)$ | $\dfrac{((C_P)_1\times m_1)+((C_P)_2\times m_2)}{m_1+m_2}$ |
| Solid volume fraction of the first nanoparticle $(\phi_1)$ | $\dfrac{\frac{m_1}{\rho_1}}{\frac{m_1}{\rho_1}+\frac{m_2}{\rho_2}+\frac{m_f}{\rho_f}}$ |
| Solid volume fraction of the second nanoparticle $(\phi_2)$ | $\dfrac{\frac{m_2}{\rho_2}}{\frac{m_1}{\rho_1}+\frac{m_2}{\rho_2}+\frac{m_f}{\rho_f}}$ |
| Equivalent volume fraction of nanoparticles $(\phi_e)$ | $\dfrac{\frac{m_1}{\rho_1}+\frac{m_2}{\rho_2}}{\frac{m_1}{\rho_1}+\frac{m_2}{\rho_2}+\frac{m_f}{\rho_f}}$ |

in which $(\rho C_P)_s = (\rho_s)(C_P)_s$ and $(\rho C_P)_f = (\rho_f)(C_P)_f$. Also the converted boundary equations can be written as follows:

$$f(c) = \frac{c\lambda}{2}, \qquad \frac{df}{d\eta}(c) = \frac{\lambda}{2}, \qquad \theta(c) = 1, \tag{8}$$

$$\frac{df}{d\eta}(\infty) \to \frac{1-\lambda}{2}, \qquad \theta(\infty) \to 0. \tag{9}$$

where the magnetic parameter $(M)$, the similarity radius of the slim needle $(c)$, the velocity ratio parameter $(\lambda)$, the radiation parameter $(R)$ and the Prandtl number $(Pr)$ are defined as:

$$M = \frac{\sigma B_0^2 x}{2\rho_f U_0}, \qquad c = \frac{U_0 R(x)^2}{\upsilon_f x}, \qquad \lambda = \frac{u_w}{U_0}, \qquad R = \frac{16\sigma^* T_\infty^3}{3K^* k_f}, \qquad Pr = \frac{\upsilon_f}{\alpha_f}. \tag{10}$$

It should be noted that $U_0 = u_w + U_\infty$. Furthermore, we set $\eta = c$ and obtain the function of the needle radius as $R(x) = \{(\upsilon_f\, cx) / (U_0)\}^{0.5}$. In addition, we consider the special cases as i) $\lambda = 0$ (Blasius flow), $\lambda = 1$ (Sakiadis flow), $0 < \lambda < 1$ (both free stream and needle move towards the positive $x$-direction) and $-1 < \lambda < 0$ (free stream moves the right side, while the needle moves the left side).

The skin friction coefficient $(C_f)$ and the local Nusselt number $(Nu_x)$ are introduced as (Soid et al., 2017):

$$C_f = \frac{\mu_{hnf}\left(\dfrac{\partial V_x}{\partial r}\right)_{r=R(x)}}{\rho_f U_0^2}, \qquad\qquad Nu_x = \frac{-x k_{hnf}\left(\dfrac{\partial T}{\partial r}\right)_{r=R(x)}}{k_f (T_w - T_\infty)}. \tag{11}$$

Finally putting Eq. (11) into Eq. (5), results in

$$C_f\left[Re_x\right]^{0.5} = 4c^{0.5}\left(1 - \frac{\dfrac{m_1}{\rho_1} + \dfrac{m_2}{\rho_2}}{\dfrac{m_1}{\rho_1} + \dfrac{m_2}{\rho_2} + \dfrac{m_f}{\rho_f}}\right)^{-2.5} \frac{d^2 f}{d\eta^2}(c), \tag{12}$$

$$Nu_x\left[Re_x\right]^{-0.5} = -2c^{0.5}\frac{k_{hnf}}{k_f}\frac{d\theta}{d\eta}(c).$$

where $Re_x = (U_0 x) / (\upsilon_f)$ is the local Reynolds number.

## 3. Results and discussion

The boundary value problem given in Eqs. (6)-(9) has been numerically solved using the function bvp4c from MATLAB for different values of the involved parameters $M$, $R$, $Pr$, $c$, $\lambda$, $m_1$, $m_2$, $m_f$, $\rho_s$ and $(C_P)_s$. In order to apply the bvp4c routine we have to rewrite our boundary value problem as systems of first-order ODEs. The function bvp4c is a finite difference code that implements the 3-stage Lobatto IIIa formula. This is a collocation formula and the collocation polynomial gives us a $C^1$-continues solution which is forth-order accurate uniformly in the interval where the function is integrated (Roşca et al., 2016; Shampine et al., 2003). In this approach, we have chosen a suitable finite value of $\eta_{max}$ between 9 and 17, where the relative tolerance was set at $10^{-6}$. Mesh selection and error control are based on the residual of the continues solution. Moreover, the first solutions are always easily obtain with even poor initial guesses. But, it is hard to determine a relevant initial guess to obtain the second solutions of the governing ODEs (6) and (7) subject to the boundary conditions (8) and (9). So, we changed the initial guesses more and more until we get the correct answers that are able to satisfy the boundary conditions.

Table 3 is presented to compare $d^2f / d\eta^2(c) = f''(c)$ for pure water without magnetic field and thermal radiation effects when $m_f = 100gr$, with previous results obtained by Ishak et al. (2007), Soid et al. (2017) and Hamid et al. (2019). As can be seen in Table 3, a very excellent agreement can be observed between them. Also, it can be deduced that the mass-based model proposed here is an efficient algorithm for analyzing the hybrid nanofluid's problems with great confidence.

**Table 3.** Validation of the present article for $f''(c)$ when $M = R = m_1 = m_2 = \phi_1 = \phi_2 = 0$, $m_f = 100gr$.

| | $\lambda = 0$ | | $\lambda = -1$ | | | | | | | |
| | Hamid et al. (2019) | Present study | Soid et al. (2017) | | Ishak et al. (2007) | | Hamid et al. (2019) | | Present study | |
| $c$ | | | First solution | Second solution | First solution | Second solution | First solution | Second solution | First solution | Second solution |
|---|---|---|---|---|---|---|---|---|---|---|
| 0.001 | – | 62.1612 | – | – | 197.2699 | 22.0693 | – | – | 196.9878 | 22.0688 |
| 0.01 | 8.4988157 | 8.49217 | 26.599394 | 2.805533 | 26.6021 | 2.8031 | 26.601911 | 2.804354 | 26.5994 | 2.8028 |
| 0.1 | 1.2914272 | 1.28907 | 3.703713 | 0.389103 | 3.7162 | 0.3884 | 3.7043034 | 0.387491 | 3.7037 | 0.3877 |
| 0.2 | 0.7540276 | 0.75193 | 2.005424 | 0.227837 | – | – | 2.0061851 | 0.225739 | 2.0054 | 0.2202 |

Figures 2 and 3, in turn illustrate the variation of $f''(c)$ and $-d\theta / d\eta(c) = -\theta'(c)$ with the velocity ratio parameter ($\lambda$), for several values of the magnetic parameter ($M$) when $m_1 = m_2 = 20gr$, $m_f = 100gr$, $c = R = 0.1$ and $Pr = 6.2$. These figures show that dual solutions (i.e. the upper solution branch and the lower solution branch) exist for the boundary value problem (Eqs. (6)-(9)) when the slim needle moves in the opposite direction of the free stream ($\lambda_c < \lambda < 0$). Further, the magnetic parameter limits the range of $\lambda$ for which the solution exists. Also $\lambda_c$ is the critical value of $\lambda$ beyond which similarity Eqs. (6) and (7) have no solutions. Besides, when both the slim needle and the free stream move to the right side ($0 < \lambda < 1$), we have a unique solution. In addition, only the first solutions are physically realizable and stable and they are always possess thinner thicknesses relative to the second solutions. Figure 4 demonstrates the samples of dimensionless velocity ($f'(\eta)$) and temperature ($\theta(\eta)$) profiles for several values of $M$ when $m_1 = m_2 = 15gr$, $m_f = 100gr$, $R = c = 0.1$, $\lambda = -3$ and $Pr = 6.2$. It should be mentioned that, the velocity profiles are the solutions which have been plotted from $f'(\eta = 0) = -1.5$ to $f'(\eta = 17) = 2$. We observe that the magnetic parameter enhancement can decrease the velocity profiles for first solutions (real solutions) due to the fact that by applying a magnetic field, the Lorentz force is applied in the opposite direction of the flow field and leads to slow down it. On the other hand, the magnetic parameter has no significant effect in temperature distributions for the first solutions. Although, it is able to dramatically enhance them for the second solutions that never happens in the real world.
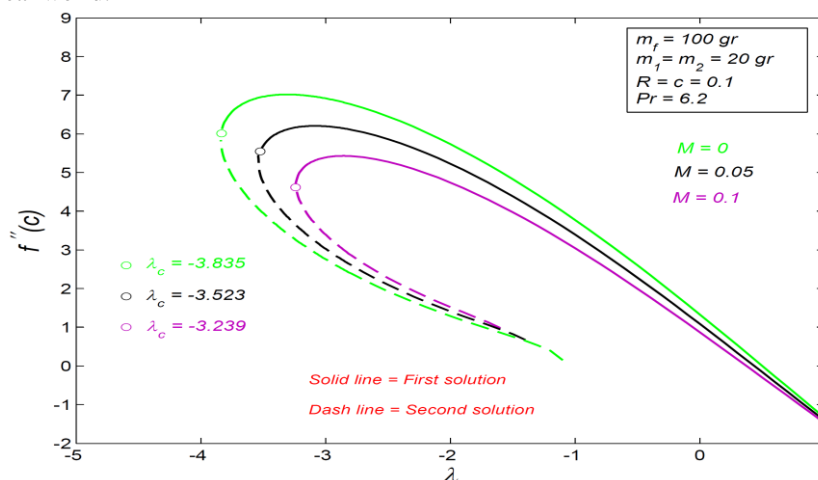


**Figure 2.** Variation of $f''(c)$ as a function of $\lambda$ for several values of $M$.
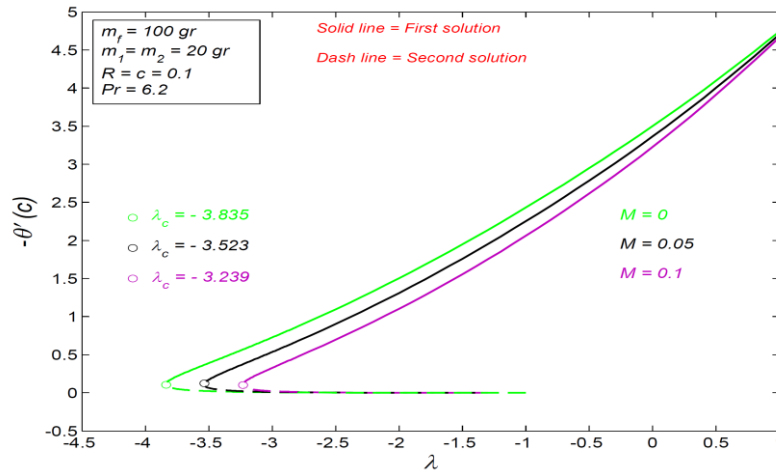
**Figure 3.** Variation of $-\theta'(c)$ as a function of $\lambda$ for several values of $M$.
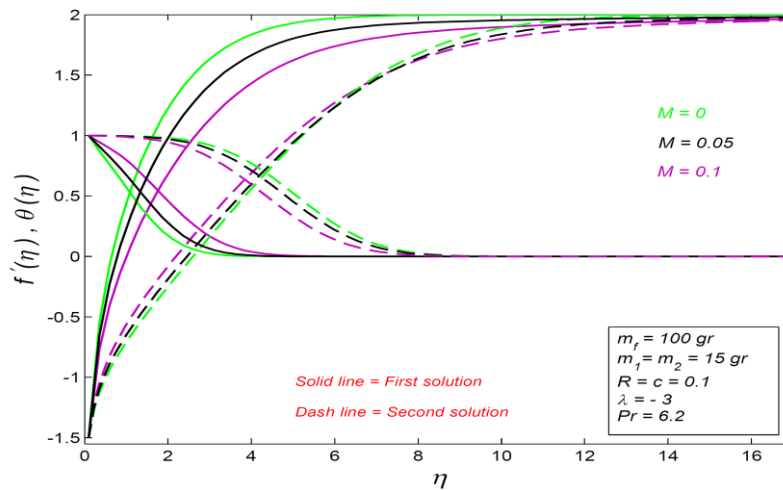


**Figure 4.** Dimensionless velocity $(f'(\eta))$ and temperature $(\theta(\eta))$ profiles for several values of $M$.

Figures 5 and 6 respectively depict the variation of $f''(c)$ and $-\theta'(c)$ with the velocity ratio parameter ($\lambda$), for several values of the second nanoparticle's mass $(m_2)$, when $m_1 = 20gr$, $m_f = 100gr$, $M = 0.15$, $R = c = 0.1$ and $Pr = 6.2$. Once again, we clearly can see that the dual solutions exist for $\lambda_c < \lambda < 0$. Furthermore, $m_2$ decreases the range of $\lambda$ for which the solution exists. The samples of $f'(\eta)$ and $\theta(\eta)$ profiles for several values of $m_2$ has been shown in Fig. 7, when $m_1 = 15gr$, $m_f = 100gr$, $M = 0.15$, $R = c = 0.1$, $\lambda = -3$ and $Pr = 6.2$. The velocity profiles are the solutions which have been plotted from $f'(\eta = 0) = -1.5$ to $f'(\eta = 17) = 2$. It is implied that the velocity profiles tend to increase for both first and second solutions by adding the second nanoparticle's mass in the advanced working fluid, while the opposite trend is true for the temperature profiles. As a consequence, $m_2$ has a positive impact on the present study so that it leads to decrease the thermal boundary layer thickness which affects the heat transfer rate enhancement.
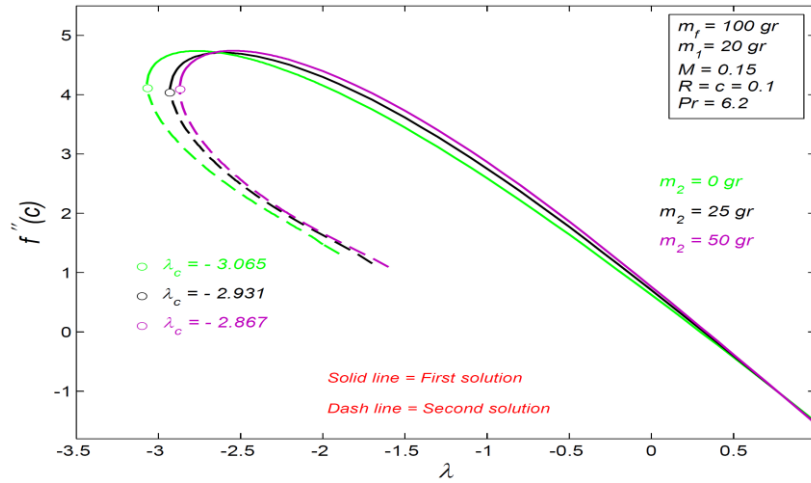
**Figure 5.** Variation of $f''(c)$ as a function of $\lambda$ for several values of $m_2$.
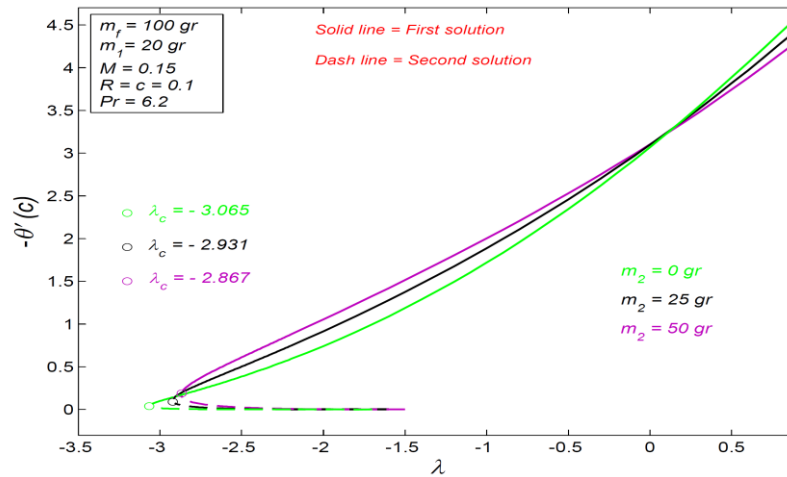


**Figure 6.** Variation of $-\theta'(c)$ as a function of $\lambda$ for several values of $m_2$.
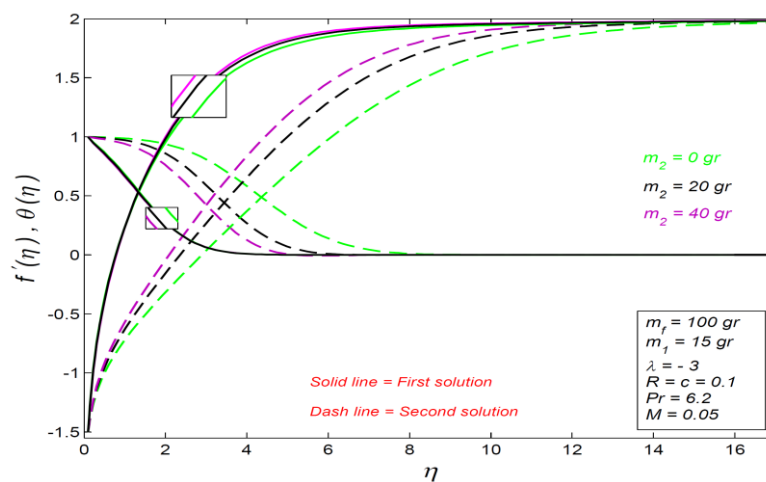


**Figure 7.** Dimensionless velocity $(f'(\eta))$ and temperature $(\theta(\eta))$ profiles for several values of $m_2$.

Figure 8 presents the samples of $\theta(\eta)$ profiles for several values of the thermal radiation parameter $(R)$, when $m_1 = m_2 = 15 gr$, $m_f = 100 gr$, $M = 0.15$, $c = 0.1$, $\lambda = -3$ and $Pr = 6.2$. It is quiet clear that the

thermal radiation parameter results in augment the thermal boundary layer thicknesses for both first and second solutions. Also, there is a point at the middle of the thermal boundary layers for both first and second solutions where the temperature attains the same value for all values of $R$. In fact, before this cross point, the temperature diminishes with $R$, while the opposite trend is valid for after this cross point.
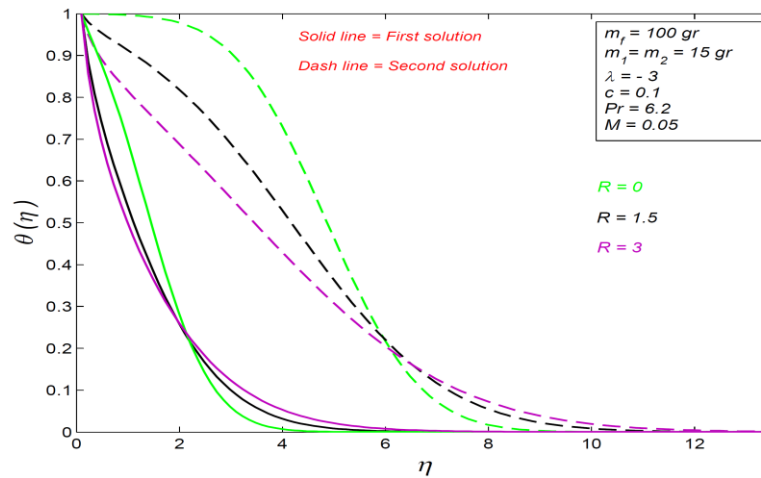


**Figure 8.** Dimensionless temperature $(\theta(\eta))$ profiles for several values of $R$.

## 4. Conclusions

A theoretical study has been presented for the flow of a hybrid nanofluid past a horizontal moving slim needle in the presence of thermal radiation with dual solutions analysis. The outcomes of the present study can be explained as: 1) the dual solutions of the problem are obtained only for $\lambda_c < \lambda < 0$, 2) the first solutions has always thinner than the second solutions, 3) the first solutions (the upper branch solutions) occur in real world and physically realizable, 4) the magnetic parameter $(M)$ and also the second nanoparticle's mass $(m_2)$ limit the range of $\lambda$ for which the solution exists, 5) the radiation parameter $(R)$ only affects the thermal characteristics of the problem because it appears directly in the similarity energy equation (see Eq. (7)), 6) the mass-based model can be successfully used for analyzing hybrid nanofluids in different problems with great confidence.

## References

Che Sidik, N.A., Muhammad Adamu, I., Jamil, M.M., Kefayati, G.H.R., Mamat, R., & Najafi, G. (2016). Recent progress on hybrid nanofluids in heat transfer applications: A comprehensive review. International Communications in Heat and Mass Transfer, 78, 68–79.

Dinarvand, D. (2019). Nodal/saddle stagnation-point boundary layer flow of CuO–Ag/water hybrid nanofluid: a novel hybridity model. Microsystem Technologies, 25, 2609–2623.

Dinarvand, S., & Nademi Rostami, M. (2019). An innovative mass-based model of aqueous zinc oxide–gold hybrid nanofluid for von Kármán's swirling flow. Journal of Thermal Analysis and Calorimetry, 138, 845–855.

Dinarvand, S., Nademi Rostami, M., & Pop, I. (2019). A novel hybridity model for TiO2-CuO/water hybrid nanofluid flow over a static/moving wedge or corner. Scientific Reports, 9, 16290.

Dinarvand, S., Nademi Rostami, M., Dinarvand, R., & Pop, I. (2019). Improvement of drug delivery micro-circulatory system with a novel pattern of CuO-Cu/blood hybrid nanofluid flow towards a porous stretching sheet. International Journal of Numerical Methods for Heat & Fluid Flow, 29, 4408-4429.

Ghadikolaei, S.S., Yassari, M., Sadeghi, H., Hosseinzadeh, K., & Ganji, D.D. (2017). Investigation on thermophysical properties of TiO2–Cu/H2O hybrid nanofluid transport dependent on shape factor in MHD stagnation point flow. Powder Technology, 322, 428–438.

Gupta, M., Singh, V., Kumar, S., Kumar, S., Dilbaghi, N., & Said, Z. (2018). Up to date review on the synthesis and thermophysical properties of hybrid nanofluids. Journal of Cleaner Production, 190, 169–192.

Hamid, A., Hashim, A., Hafeez, M., Khan, A.S., & Alshomrani, M. (2019). Heat transport features of magnetic water–graphene oxide nanofluid flow with thermal radiation: Stability Test. European Journal of Mechanics / B Fluids, 76, 434–441.

Hamzah, M.H., Nor Azwadi Che Sidik, T.L., Ken, R., Mamat, G., & Najafi, F. (2017). Factors affecting the performance of hybrid nanofluids: A comprehensive review. International Journal of Heat and Mass Transfer, 115, 630–646.

Ijaz, S., Iqbal, Z., Maraj, E.N., & Nadeem, S. (2018). Investigation of Cu-CuO/blood mediated transportation in stenosed artery with unique features for theoretical outcomes of hemodynamics. Journal of Molecular Liquids, 254, 421–432.

Ishak, I., Nazar, R., & Pop, T. (2007). Boundary layer flow over a continuously moving thin needle in a parallel free stream. Chinese Physics Letters, 24, 2895–2897.

Khashi'ie, N.S., Md Arifin, N., Pop, I., Nazar, R., Hafidzuddin, E.H., & Wahi, N. (2020). Flow and heat transfer past a permeable power-law deformable plate with orthogonal shear in a hybrid nanofluid. Alexandria Engineering Journal, 59, 1869–1879.

Lee, L.L. (1967). Boundary layer over a thin needle. Physics of Fluids, 10, 820–822.

Madhesh, D., & Kalaiselvam, S. (2014). Experimental Analysis of Hybrid Nanofluid as a Coolant. Procedia Engineering, 97, 1667 – 1675.

Moldoveanua, G.M., Mineaa, A.A., Iacob, M., Ibanescu, C., & Danu, M. (2018). Experimental study on viscosity of stabilized Al2O3, TiO2 nanofluids and their hybrid. Thermochimica Acta, 659, 203–212.

Roşca, N.C., Roşca, A.V., Aly, E.H., & Pop, I. (2016). Semi-analytical solution for the flow of a nanofluid over a permeable stretching/shrinking sheet with velocity slip using Buongiorno mathematical model. European Journal of Mechanics B/Fluids, 58, 39–49.

Sarkar, J., Ghosh, P., & Adil, A. (2015). A review on hybrid nanofluids: Recent research, development and applications. Renewable and Sustainable Energy Reviews, 43, 164–177.

Shampine, L.F., Gladwell, I., & Thompson, S. (2003). Solving ODEs with MATLAB, Cambridge University Press.

Shojaie Chahregh, H., & Dinarvand, S. (2020). TiO2-Ag/blood hybrid nanofluid flow through an artery with applications of drug delivery and blood circulation in the respiratory system. International Journal of Numerical Methods for Heat & Fluid Flow, 30, 4775-4796.

Soid, S.K., Ishak, A., & Pop, I. (2017). Boundary layer flow past a continuously moving thin needle in a nanofluid. Applied Thermal Engineering, 114, 58–64.

Tiwari, R.J., & Das, M.K. (2007). Heat transfer augmentation in a two sided lid-driven differentially heated square cavity utilizing nanofluids. International Journal of Heat and Mass Transfer, 50, 2002–2018.

Upreti, H., & Kumar, M. (2019). Influence of non-linear radiation, Joule heating and viscous dissipation on the boundary layer flow of MHD nanofluid flow over a thin moving needle. Multidiscipline Modeling in Materials and Structures, 16, 208-224.

Yousefi, M., Dinarvand, S., Eftekhari Yazdi, M., & Pop, I. (2018). Stagnation-point flow of an aqueous titania-copper hybrid nanofluid toward a wavy cylinder. International Journal of Numerical Methods for Heat & Fluid Flow, 28, 1716-1735.